

# A MODIFICATION TO THE ASM FILTER FOR IMPROVING SAR INTERFEROGRAMS

Wajih Ben Abdallah<sup>1</sup> and Riadh Abdelfattah<sup>1,2</sup>

<sup>1</sup> COSIM Lab, University of Carthage, Higher School of Communications of Tunis,  
Route de Raoued KM 3.5, Cite El Ghazala Ariana 2083 - Tunisia, wajihabdou@gmail.com

<sup>2</sup> Département ITI, Télécom Bretagne, Institut de Télécom, Technopôle Brest-Iroise CS 83818 - 29238  
Brest Cedex 3 - France, riadh.abdelfattah@supcom.rnu.tn

## ABSTRACT

SAR Interferograms illustrate an ambiguous (modulo  $2\pi$ ) and noisy phase. In this paper, we focus on the step of interferogram denoising using the Adaptive Switching Median Filter (ASMF) in the wavelet domain. Thus, we propose to filter the coefficients of the relative Discrete Packet Wavelet Transform (DPWT). Our main contribution in this paper concerns firstly, the methodology for computing the mask of noise corresponding to the InSAR phase. Secondly, the size of the median filter is computed considering the noise mask within a given neighborhood and taking into account the corresponding InSAR coherence values. This scheme is tested on simulated noisy interferograms as well as on a given pairs of single look complex (SLC) data from Envisat satellite. Validation was made by computing the Digital Elevation Model after unwrapping the filtered interferogram.

**Index Terms**— SAR Interferogram, ASM Filter, Wavelet Transform, InSAR coherence.

## 1. INTRODUCTION

The interferometric data, produced by the SAR systems, is used to measure the relief and detect any changes accrued to the surface of the earth by computing the phase difference information between two complex radar images [1]. Indeed, a phase difference image is generated using both complex images, which is named interferogram. The phase difference is proportional to the geomorphological parameters (height, displacement, ...) of the imaged terrain [1]. However, in practice the real interferogram is affected by an additive noise and a various decorrelation effects (thermal noise, geometrical conditions,...) [2]. In the literature, many SAR interferogram filtering algorithms were proposed, such as the Goldstein filter [3], the weighted filter [4], the Lee filter [2] and the adaptive window filter [5].

In the wavelet domain, López and Fabregàs proposed in [6] a new wavelet-based approach called Wavelet Interferometric Phase Filter (WInPF) to filter the SAR interferogram by using the packet wavelet transform technique with three

decomposition levels. Their main idea consists on the extracting of the useful signal from the noisy phase image by using a fixed threshold to all sub-bands wavelet coefficients [6]. However, the different sub-bands of the wavelet transform are not computed by the same way and they do not contain neither the same kind of information nor the dynamics (useful data in the low frequency bands and almost noise in the high frequency bands). So, this thresholding operation is not adapted to the high variation values of the InSAR phase. To bypass this disadvantage, Abdelfattah and Bouzid [7] proposed a new filter named Filtre par Approche Multi-échelle Modifiée (FAMM) by using the coherence map to compute an adaptive threshold and generate a more accurate noise mask. The analysis of these filter results presented in [6] and [7], shows that the filtered interferogram still having noisy pixels which appears as an impulse noise (Fig. 3 - (c)). To correct this problem, we propose, in this paper, a new process by applying the Adaptive Switching Median Filter (ASMF) [8], mainly used to eliminate the impulse noise, to filter the noisy areas in the WInP and the FAMM filter results. The ASM filter was firstly proposed by Cai and Lee [8]. It is mainly used to filter the natural images affected by the impulse noise. It gives better results than the standard median filter [9], the switching median filter [10] and the modified switching median filter [11]. Thus, to adapt the classic ASMF to the SAR interferograms, we propose in this paper an Enhanced version of the ASM filter where the size of the filtering window centred on a given pixel, depends on the number of its noise free neighbours. This could be possible using the InSAR coherence distribution in the studied neighbourhood.

This paper is organized as follows. Section 2 presents the problem of the SAR filtering with the WInP filter approach. Then, section 3 presents the interferogram noise reduction method based on the median filter and describes the classic and the enhanced versions of the ASM filter respectively. Section 4 gives the experimental results and comparisons of the proposed scheme with other filter approaches (essentially the WInP filter). A validation process is then presented in this section after an unwrapping step and DEM generation. The conclusion derived from this work is given in the last section.

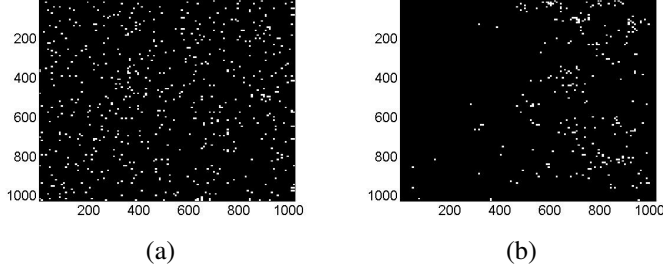


**Fig. 1.** The mask of noise (noisy pixels in white) generated by the WInPF algorithm for (a) the simulated interferogram of Fig. 3, with correlation coefficient = 0.5 and (b) the real SAR interferogram of Fig. 5.

## 2. PROBLEMATIC OF THE SAR INTERFEROGRAM FILTERING IN THE WAVELET DOMAIN

Lopéz and Fabregàs [6] are based on an additive noise model as described in [2] and they have developed an InSAR filter using the Discrete Packet Wavelet Transform (DPWT) with three decomposition levels [6]. Their main idea is to amplify the useful signal in the interferogram. To do this, they used a signal quality coefficient  $\Gamma_{sig}$  and compared it with a fixed and unique threshold  $th_w$  for all 16 sub-bands of the DPWT [6] as follows:

$$w_\epsilon = \begin{cases} \text{signal coefficient if } \Gamma_{sig} \geq th_w \\ \text{noise coefficient if } \Gamma_{sig} < th_w \end{cases} \quad (1)$$

Since these sub-bands are computed differently and the useful signal is located in the low frequency band and the noise is in the high frequency band, the unique threshold used for those sub bands often gives false decisions and therefore, the interferogram filtered by the WInPF still containing impulse noise as shown in the mask noise (Fig. 1) and the filtered interferogram (Fig. 3 (c)). For this reason, it is high recommended to use a proper threshold for each band. The more adaptive way to eliminate this kind of noise is to apply a median filter to the WInP result. But while interferometric phase images present a particular probability density function (pdf) taking into account for operating the fringe pattern filtering with the WInP filter, we propose to take advantage of this process and reduce the effect of the resulting impulse noise with a complementary processing. It consists on an enhanced version of the classic adaptive switching median filter which take into account the coherence map of the interferogram as it will be described in the next section.

## 3. MEDIAN FILTERING FOR SAR INTERFEROGRAMS

### 3.1. Adaptive Switching Median Filter

The Adaptive Switching Median Filter (ASMF) [8] is a modified version of the adaptive median filter which the size of

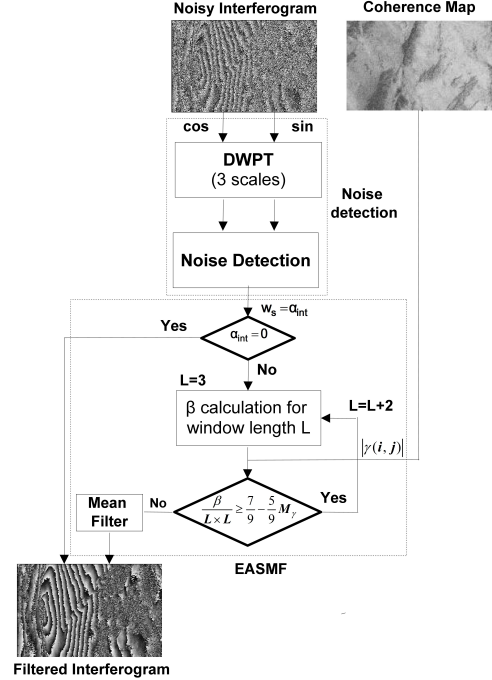


**Fig. 2.** Flowchart of the proposed EASM filter for interferometric phase denoising.

its noise cancellation window centered at a given pixel is a function of its neighbours. For each pixel  $(x, y)$  on the input image, we calculate the mask  $\alpha$  as follows [8]:

$$\alpha(x, y) = \begin{cases} 1 & \text{if } f(x, y) \text{ is a noisy pixel} \\ 0 & \text{otherwise} \end{cases} \quad (2)$$

where  $f$  is the noisy image. Then, by using this noise mask, the following value is calculated at every coordinates  $(x, y)$ :

$$\beta(x, y) = \sum_{i=x-1}^{x+1} \sum_{j=y-1}^{y+1} \alpha(i, j) \quad (3)$$

The value of  $\beta$  indicates the total number of noisy pixels within a window of size  $3 \times 3$  pixels. By using (2) and (3), the output of ASMF will be [8]:

$$f_1(x, y) = \begin{cases} f(x, y) & \text{if } \alpha(x, y) = 0 \text{ or } \beta(x, y) = 9 \\ m(x, y) & \text{otherwise} \end{cases} \quad (4)$$

Where  $m$  is the median value in the window centred on  $(x, y)$ . This filter output means that the filtered image  $f_1$  maintains the originally one in the pixel  $(x, y)$  if it is a noise free or if all their neighbours are noisy pixels. The window length  $L$  depends on the number of noisy pixels within the neighbourhood of  $(x, y)$  [8] as follows:

$$L \times L = \begin{cases} 3 \times 3 & \text{if } \beta(x, y) = 1 \\ 7 \times 7 & \text{if } \beta(x, y) = 8 \\ 5 \times 5 & \text{otherwise} \end{cases} \quad (5)$$

The idea of increasing the window length ( $L$ ) in (5) is in order to have more likely noisy free pixels in the studied neighbourhood.

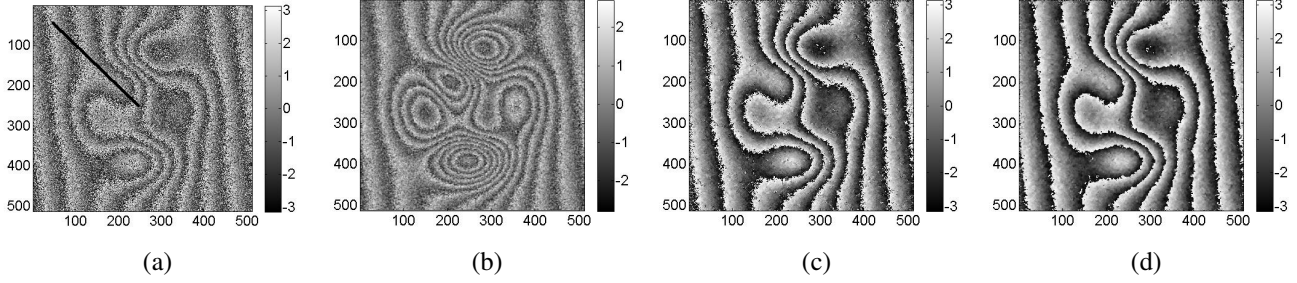


**Fig. 3.** Filtering results of the simulated interferogram (a) the original noisy phase image with correlation between two single look complex images = 0.5 (b) filtered result with the Kuan filter (c) with the WInP filter and (d) with the proposed EASMF filter.

### 3.2. Proposed Methodology : EASMF

The ASM filter is mainly used to remove the impulse noise from natural images and the pixel is considered as noisy if it take the maximum or the minimum value of intensity (0 or 255 for gray pictures) [12]. The idea to apply this filter after the step of denoising the interferogram in the wavelet packet domain is because of the result of denoising which is still affected with an impulse noise (Fig. 3 (c) and Fig. 5 (b)). However, the classical mask of noise computed within the ASM framework is not adapted to the phase context where the pixels values are between  $-\pi$  and  $+\pi$  and it is not recommended to transform the dynamic of the interferogram. In fact, this may cause more sampling error in the nterferogram. In this section, we propose two modifications to the classical ASM filter: the computation of the noise mask and the selection of the filtering window size. These are the main contributions of this paper.

To obtain the new noise mask  $\alpha_{int}$ , we combine (1) and (2):

$$\alpha_{int}(x, y) = \begin{cases} 1 & \text{if } w_\epsilon \text{ is a noise pixel} \\ 0 & \text{otherwise} \end{cases} \quad (6)$$

And (3) will become in the interferogram case:

$$\beta_{int}(x, y) = \sum_{i=x-1}^{x+1} \sum_{j=y-1}^{y+1} \alpha_{int}(i, j) \quad (7)$$

It is obvious that smaller filter size must be applied at pixel locations with low noise level in order to preserve the local data information and on the other hand, larger filter size could be preferable when higher noise level is detected. In fact, the pixels within the processed neighborhood have to be homogeneous, which is not guaranteed in case of the large size of the filtering window. We then propose to model the degree of homogeneity within the filter window as a function of the InSAR coherence value  $|\gamma|$  defined as:

$$|\gamma| = \left| \frac{E(I_1 I_2^*)}{\sqrt{E(|I_1|^2) E(|I_2|^2)}} \right| \quad (8)$$

where  $I_1$  and  $I_2$  are the two single look images of the satellite and \* denotes the conjugate value. In fact, the degree of the InSAR coherence do not only express the decorrelation effects but also the target particularities: different targets will

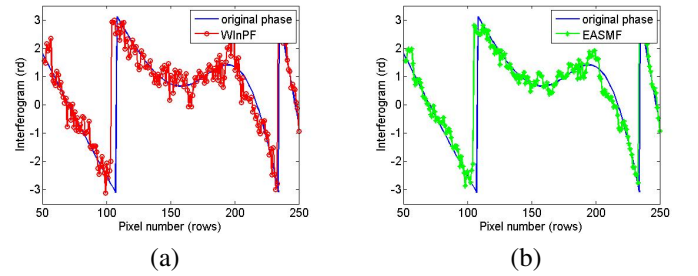


**Fig. 4.** Comparaion of the interferogram intensities change as noisy initials values and filtered along a profiler slope (black line in Fig. 3(a)) (a) filtered with WInP filter and (b) filtered with EASMF filter.

generate different degree of coherence. We will proceed as follows:

- The mean of coherence values within a  $3 \times 3$  window, centred on pixel  $(x, y)$  is computed as follows:

$$M_\gamma(x, y) = 1/9 \sum_{i=x-1}^{x+1} \sum_{j=y-1}^{y+1} |\gamma(i, j)| \quad (9)$$

- The coherence threshold  $th_{coh}$  to be used for the decision on the length of the filtering window  $L_{int}$  is computed by assuming that it varies linearly according to the coherence magnitude  $th_{coh} = a + bM_\gamma$

This threshold computes an estimation of the percentage of noisy pixels in a  $3 \times 3$ , with respect to the mean of their coherence values. To find  $a$  and  $b$ , we assume that the number of noisy pixels should not exceed 2 from the 9 pixels within a  $3 \times 3$  window if  $M_\gamma \approx 1$  and should not exceed 7 from the 9 pixels if  $M_\gamma \approx 0$ . Consequently, we replace  $|\gamma|$  by 0 and we obtain  $a = \frac{7}{9}$  and  $b = -\frac{5}{9}$ . Then the estimated threshold is given by:

$$th_{coh} = \frac{7}{9} - \frac{5}{9}M_\gamma \quad (10)$$

After computing the threshold  $th_{coh}$ , the window length  $L_{int}$  centered in  $(x, y)$  of the enhanced ASM filter will be computed with the following modified ASM algorithm, (The corresponding flowchart is given in Fig. 2):

*Step 1 : initialisation  $L_{int} = 3$*

*Step 2 : computing  $\beta_{int}(x, y)$  within the window of length  $L_{int}$  and centred on  $(x, y)$ ,*

*Step 3 : if  $\frac{\beta_{int}(x, y)}{L_{int}^2} > th_{coh}$  then  $L_{int} = L_{int} + 2$ , break otherwise,*

*Step 4 : repeat step 2 and step 3 until  $L_{int} = 7$ .*

Finally, the output of EASM filter will be:

$$\hat{\phi}(x, y) = \begin{cases} \phi(x, y) & \text{if } \alpha_{int} = 0 \\ m_{int}(x, y) & \text{otherwise} \end{cases} \quad (11)$$

where  $\phi$  and  $\hat{\phi}$  are the initial and the filtered phase respectively and  $m_{int}(x, y)$  is the median value within the window of length  $L_{int}$  and centred on  $(x, y)$ . In next section, we propose to validate the filtered interferogram through on unwrapping of  $\hat{\phi}$  phase given in (11).

#### 4. EXPERIMENTAL RESULTS AND DISCUSSIONS

We used in this paper two kinds of interferograms: the first one is a simulated interferogram with Matlab by wrapping a 3D relief model generated by the meshgrid and peaks functions. This interferogram is  $512 \times 512$  pixels size and with phase values varying between  $-\pi$  and  $+\pi$ . The second one is derived from a single look complex pair (SLC) of Envisat satellite acquired over Etna mountain in Italy and supplied with the NEST software [13]. Note that for Kuan filter [14] and WInPF filter [6] we used the same values of the parameters as described in their original papers  $th_w = -5$ . For the simulated interferogram, we used a correlation value  $|\rho| = 0.5$  between the two complex images (Fig. 3). For both kinds of interferograms, the visual analysis shows that the proposed filter reduce more the impulse noise presented in the WInPF output interferogram, as shown in (Fig. 3 (c) and Fig. 5 (b)). Moreover, the fringe edges are not smoothed for both the WInP and EASM filters. For the quantitative study, we compute the Normalized Mean Square Error (NMSE) between the simulated interferogram filtered by the Kuan [14], the WInP, the FAMM [7] and EASM filters respectively and the original interferogram without noise. The comparison between the different MSE is given in Table 1, where we can note that the EASM filter gives the optimal results.

We also computed the image cut filtering results of the black line shown in Fig. 3 and we can notice that the graph phase given by EASM filter is almost close to the original one without noise (Fig. 4). These results of the EASM filter are still taking place in the case of the real iterferogram. We used

**Table 1.** Normalized Mean Square Error computed using different filtering algorithm on a  $512 \times 512$  simulated phase image given different correlation values.

$ \rho $	Kuan	WInPF	FAMM	EASMF
0.5	0.664	0.220	0.249	<b>0.210</b>
0.7	0.499	0.126	0.129	<b>0.123</b>
0.9	0.174	0.068	0.067	<b>0.066</b>

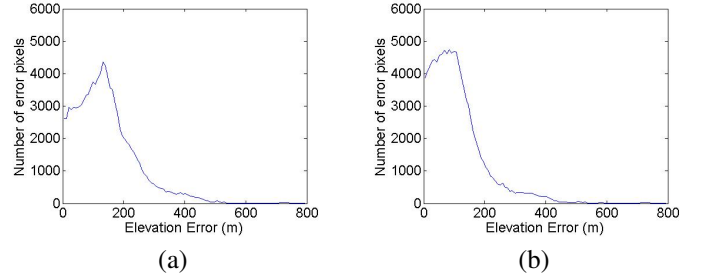


**Fig. 6.** The distribution histogram of the elevation error between the real DEM provided from ASTER satellite and the DEM produced from the filtered unwrapped phase using (a) the WInP filter and (b) the EASM filter.

in this paper a part of the whole interferometric phase image with size  $1024 \times 1024$ , given from a pair of SLC data produced by the Envisat satellite acquired over the Etna mountain in Italy on 1 and 2 August 1995 respectively with a baseline of 61.36 m between each acquisition. After filtering with the WInP filter, the impulse noise is still apparent in many areas of the filtered interferogram and it hasn't been filtered (Fig. 5 (b)) but most of them have been detected and filtered by the developed approach (Fig. 5 (c)). Thus, we can see that the fringe edges in the proposed filter output were preserved perfectly. After computing the filtered InSAR image, and to validate the proposed approach on the real data too, we computed the unwrapped filtered real interferogram. To obtain the unwrapped phase, we used the Quality-Guided phase unwrapping algorithm described in [15]. After applying the unwrapping process, we computed the Digital Elevation Model (DEM) from the unwrapped filtered phase and compared it with the real DEM of the same acquired region. We used in this paper the ASTER Global DEM available in the Land Processes Distributed Active Archive Center website at a spatial resolution of 30 meters. The histograms of the absolute error between the real DEM and the filtered ones with WInPF and EASMF respectively are shown in Fig. 6 ((a) - (b)). We notice that 89.08% of pixels filtered with the EASM filter have an elevation error between 0 and 200 meters, while only 87.84% of pixels in the case of WInP filter.

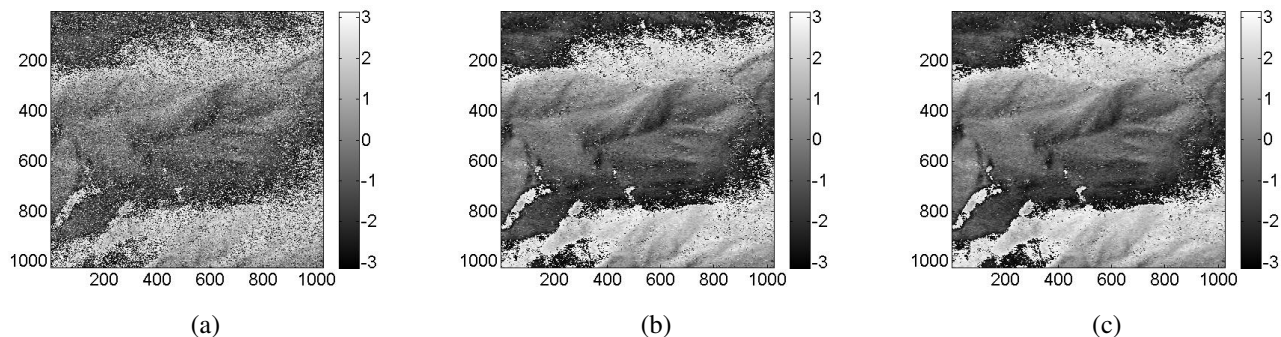


**Fig. 5.** Filtering results of a  $1024 \times 1024$  pixels size part of the full Envisat interferogram : (a) the original interferogram, (b) filtered by WInPF (c) and filtered by EASMF.

## 5. CONCLUSION

In this paper, we presented an enhanced version of the ASM filter based on the wavelet transform. The main idea of this approach is to generate the noise mask by using the InSAR coherence map to adjust the size of the noise cancellation window. The filtered interferogram is validated by computing the unwrapping phase with Quality-Guided method [15] and comparing the NMSE of the filtered phase image with WInP and Kuan filter one's. The developed approach gives a better result with respect to these filters. Also, the proposed method was tested with real data interferograms using SLC data acquired with the Envisat Satellite over the Etna mountain on August 1995. The proposed algorithm eliminates most of the noise remaining in the WInPF output image.

## 6. REFERENCES

- [1] R. Abdelfattah and J. M. Nicolas, "Topographic sar interferometry formulation for high-precision dem generation," *IEEE Trans. Geosci and Remote Sensing*, vol. 40, no. 11, pp. 2415–2426, 2002.
- [2] J. S. Lee, K. P. Papathanassiou, T. L. Ainsworth, M. R. Grunes, and A. Reigber, "A new technique for noise filtering of sar interferometric phase images," *Geoscience and Remote Sensing, IEEE Transactions on*, vol. 36, no. 5, pp. 1456–1465, 1998.
- [3] R. M. Goldstein and C. L. Werner, "Radar interferogram filtering for geophysical applications," *Geophysical Research Letters*, vol. 25, no. 21, pp. 4035–4038, 1998.
- [4] K. Q. DUAN, J. B. XIANG, and F. WANG, "An algorithm of weighted periodic pivoting median filtering for insar phase fringe [j]," *Journal of Air Force Radar Academy*, vol. 1, pp. 001, 2005.
- [5] W. Liu and G. Liu, "Insar periodic median adaptive filtering algorithm based on the phase frequency credibility," in *Image and Signal Processing (CISP), 2011 4th International Congress*. IEEE, 2011, vol. 3, pp. 1628–1632.
- [6] C. Lopez-Martinez and X. Fabregas, "Modeling and reduction of sar interferometric phase noise in the wavelet domain," *Geoscience and Remote Sensing, IEEE Transactions on*, vol. 40, no. 12, pp. 2553–2566, 2002.
- [7] R. Abdelfattah and A. Bouzid, "Sar interferogram filtering in the wavelet domain using a coherence map mask," in *Image Processing, 2008. ICIP 2008. 15th IEEE International Conference on*. IEEE, 2008, pp. 1888–1891.
- [8] Z. Cai and T. KM Lee, "Adaptive switching median filter," in *Information, Communications and Signal Processing, 2009. ICICS 2009. 7th International Conference on*. IEEE, 2009, pp. 1–4.
- [9] M. Stork, "Median filters theory and applications," in *Third International Conference on Electrical and Electronics Engineering Papers-Chamber of Electrical Engineering, Bursa, Turkey, December, 2003*, pp. 3–7.
- [10] T. Sun and Y. Neuvo, "Detail-preserving median based filters in image processing," *Pattern Recognition Letters*, vol. 15, no. 4, pp. 341–347, 1994.
- [11] S. Zhang and M. A Karim, "A new impulse detector for switching median filters," *Signal Processing Letters, IEEE*, vol. 9, no. 11, pp. 360–363, 2002.
- [12] I. Haidi, "Adaptive switching median filter utilizing quantized window size to remove impulse noise from digital images," *Asian Transactions on Fundamentals of Electronics, Communication and Multimedia*, vol. 2, no. 1, pp. 1–6, 2012.
- [13] <http://nest.array.ca/> Next ESA, "All rights reserved ," 2013.
- [14] DARWINT Kuan, ALEXANDERA Sawchuk, TIMOTHYC Strand, and PIERRE Chavel, "Adaptive restoration of images with speckle," *Acoustics, Speech and Signal Processing, IEEE Transactions on*, vol. 35, no. 3, pp. 373–383, 1987.
- [15] H. Zhong, J. Tang, S. Zhang, and M. Chen, "An improved quality-guided phase-unwrapping algorithm based on priority queue," *Geoscience and Remote Sensing Letters, IEEE*, vol. 8, no. 2, pp. 364–368, 2011.